



Research article

Kyle E. Ballantine and Janne Ruostekoski*

Parity-time symmetry and coherent perfect absorption in a cooperative atom response

<https://doi.org/10.1515/nanoph-2020-0635>

Received December 2, 2020; accepted December 31, 2020;
published online January 20, 2021

Abstract: Parity-Time (\mathcal{PT}) symmetry has become an important concept in the design of synthetic optical materials, with exotic functionalities such as unidirectional transport and nonreciprocal reflection. At exceptional points, this symmetry is spontaneously broken, and solutions transition from those with conserved intensity to exponential growth or decay. Here, we analyze a quantum-photonic surface formed by a single layer of atoms in an array with light mediating strong cooperative many-body interactions. We show how delocalized collective excitation eigenmodes can exhibit an effective \mathcal{PT} symmetry and nonexponential decay. This effective symmetry is achieved in a passive system without gain by balancing the scattering of a bright mode with the loss from a subradiant dark mode. These modes coalesce at exceptional points, evidenced by the emergence of coherent perfect absorption where coherent incoming light is perfectly absorbed and scattered only incoherently. We also show how \mathcal{PT} symmetry can be generated in total reflection and by balancing scattering and loss between different polarizations of collective modes.

Keywords: cold atoms; cooperative response; exceptional points; metasurfaces; optical lattices; \mathcal{PT} symmetry.

1 Introduction

The search for novel and powerful methods to control light using artificially engineered optical properties is a current driving force in photonics [1]. The possibility of exploiting

gain and loss in photonic systems has led to interest in combined time and parity (\mathcal{PT}) symmetries [2–4]. Applications of \mathcal{PT} symmetric systems include, e.g., nonreciprocal light propagation [5, 6], unidirectional invisibility [7, 8], and coherent perfect absorption (CPA) [9–11]. They stem from a real eigenvalue spectrum [12] that undergoes spontaneous \mathcal{PT} symmetry breaking at exceptional points (EPs) where eigenmodes coalesce and eigenvalues become complex [13]. Precise balance of gain and loss is technically challenging and effective \mathcal{PT} symmetries in passive systems are of increasing interest [3, 14, 15]. In particular, incident waves can be exploited as an effective gain such that the balance between scattering and absorption loss creates \mathcal{PT} symmetry [16, 17].

Metasurfaces [18] are thin nanostructured films of typically subwavelength-sized scatterers for the manipulation, detection, and control of light. Placing cold atoms in a two-dimensional (2D) planar array, e.g., by an optical lattice with unit occupancy has been proposed as a nanophotonic atom analogy to a metasurface [19], consisting of essentially point-like quantum scatterers. Transmission resonance narrowing due to giant Dicke subradiance below the fundamental quantum limit of a single-atom linewidth was recently experimentally observed [20] for a planar atom array, where all the atomic dipoles oscillated in phase, while incident fields can drive giant subradiance also in resonator metasurfaces [21]. These quantum-photonic [22] surfaces of atoms that have no dissipative losses due to absorption have several advantages over artificial resonator metasurfaces (even over low-dissipation all-dielectric ones [22]), as they could naturally operate in a single-photon limit [23–31], every atom has well-defined resonance parameters, and nonlinear response [32, 33] is easily achievable.

Here we show how the many-body dynamics of strongly coupled atoms in a planar array, with the dipole-dipole interactions mediated by resonant light, can be engineered to exhibit CPA, associated with an effective \mathcal{PT} symmetry breaking. By controlling atomic level shifts (e.g., by ac Stark shifts due to lasers), a collective analogue of electromagnetically induced transparency (EIT) can be constructed [34] by coupling light dominantly only to two uniform collective excitation modes: a “bright mode”, with

*Corresponding author: Janne Ruostekoski, Department of Physics, Lancaster University, Lancaster, LA1 4YB, UK, E-mail: j.ruostekoski@lancaster.ac.uk. <https://orcid.org/0000-0002-2419-9961>

Kyle E. Ballantine, Department of Physics, Lancaster University, Lancaster, LA1 4YB, UK, E-mail: k.ballantine@lancaster.ac.uk. <https://orcid.org/0000-0001-7197-0942>

atomic dipoles coherently oscillating in phase in the plane of the array, and a “dark mode”, with the dipoles oscillating in phase perpendicular to the plane. As in a standard independent-atom EIT [35], the bright and dark modes couple strongly and weakly to radiation, respectively. However, here the microscopic origin of the dark mode is not single-atom interference, but collective many-body subradiance. We show that by balancing the loss of the dark mode with the scattering of the bright mode, the system becomes invariant to \mathcal{PT} reversal. The collective eigenmodes of the system, which are linear combinations of the in-plane and out-of-plane modes, can then coalesce at the EPs, leading to spontaneous breaking of the \mathcal{PT} symmetry of the eigenvectors, realizing CPA, where coherent incoming light is perfectly absorbed and scattered only incoherently. The process can be qualitatively described by a simple two-mode model where only the two dominant collective modes are included. We also demonstrate \mathcal{PT} symmetry in other effective models of the system, related to total reflection as well as balanced scattering and loss between different polarizations of collective modes.

2 Atom light coupling

2.1 Basic relations

Our model consists of a square array of cold atoms, in the yz plane, with one atom per lattice site, and lattice constant d . The dipole moment of atom j is $\mathbf{d}_j = \mathcal{D} \sum_{\sigma} \mathcal{P}_{\sigma}^{(j)} \hat{\mathbf{e}}_{\sigma}$, where \mathcal{D} is the reduced dipole matrix element, and $\mathcal{P}_{\sigma}^{(j)}$ and $\hat{\mathbf{e}}_{\sigma}$ are the polarization amplitude and the unit vector associated with the assumed $|J=0\rangle \rightarrow |J'=1, m=\sigma\rangle$ transition, respectively.¹ We take the level detunings of this transition to be controllable, as could be achieved by ac Stark shifts of lasers or microwaves [36], or by magnetic fields. In the limit of low light intensity, the polarization amplitudes obey [37]

$$\frac{d}{dt} \mathcal{P}_{\sigma}^{(j)} = (i\Delta_{\sigma} - \gamma) \mathcal{P}_{\sigma}^{(j)} + i \frac{\xi}{\mathcal{D}} \hat{\mathbf{e}}_{\sigma}^* \cdot \epsilon_0 \mathbf{E}_{\text{ext}}(\mathbf{r}_j), \quad (1)$$

where $\Delta_{\sigma} = \omega - \omega_{\sigma}$ is the detuning of the transition to level σ from the laser frequency $\omega = ck$, $\gamma = \mathcal{D}^2 k^3 / 6\pi \hbar \epsilon_0$ is the single-atom Wigner–Weisskopf linewidth, and $\xi = 6\pi\gamma/k^3$. The electric field consists of the incident light

$\mathcal{E}(\mathbf{r}) = \mathcal{E}(y, z) \hat{\mathbf{e}}_y e^{ikx}$ and the sum of the scattered light from all other atoms, $\mathbf{E}_{\text{ext}}(\mathbf{r}_j) = \mathcal{E}(\mathbf{r}_j) + \mathbf{E}_s(\mathbf{r}_j)$, with

$$\epsilon_0 \mathbf{E}_s(\mathbf{r}_j) = \sum_{k \neq j} \mathbf{G}(\mathbf{r}_j - \mathbf{r}_k) \mathbf{d}_k. \quad (2)$$

Here, \mathbf{G} is the standard dipole radiation kernel such that the scattered field at a point \mathbf{r} from a dipole \mathbf{d} at the origin is given by (for $r = |\mathbf{r}|$, $\hat{\mathbf{r}} = \mathbf{r}/r$)

$$\mathbf{G}(\mathbf{r}) \mathbf{d} = \frac{\mathbf{d} \delta(\mathbf{r})}{3} + \frac{k^2 e^{ikr}}{4\pi} \left\{ (\hat{\mathbf{r}} \times \mathbf{d}) \times \hat{\mathbf{r}} \frac{1}{kr} - [3\hat{\mathbf{r}}(\hat{\mathbf{r}} \cdot \mathbf{d}) - \mathbf{d}] \times \left[\frac{i}{(kr)^2} - \frac{1}{(kr)^3} \right] \right\}. \quad (3)$$

Inserting \mathbf{E}_{ext} into Equation (1) leads to a set of coupled equations for the polarization amplitudes [37],

$$\begin{aligned} \frac{d}{dt} \mathcal{P}_{\sigma}^{(j)} &= (i\Delta_{\sigma}^{(j)} - \gamma) \mathcal{P}_{\sigma}^{(j)} + i\xi \sum_{k \neq j} \mathcal{G}_{\sigma\tau}^{(jk)} \mathcal{P}_{\tau}^{(k)} \\ &+ i \frac{\xi}{\mathcal{D}} \hat{\mathbf{e}}_{\sigma}^* \cdot \epsilon_0 \mathcal{E}(\mathbf{r}_j), \end{aligned} \quad (4)$$

where $\mathcal{G}_{\sigma\tau}^{(jk)} = \hat{\mathbf{e}}_{\sigma}^* \cdot \mathbf{G}(\mathbf{r}_j - \mathbf{r}_k) \hat{\mathbf{e}}_{\tau}$. These can be cast in matrix form by writing the polarization amplitudes as $b_{3\sigma+j-1} = \mathcal{P}_{\sigma}^{(j)}$, and the drive as $f_{3\sigma+j-1} = i\xi \epsilon_0 \hat{\mathbf{e}}_{\sigma}^* \cdot \mathcal{E}(\mathbf{r}_j)/\mathcal{D}$ to give

$$\dot{\mathbf{b}} = i\mathcal{H} \mathbf{b} + \mathbf{f}, \quad (5)$$

where the diagonal elements $\mathcal{H}_{3\sigma+j-1, 3\sigma+j-1} = (\Delta_{\sigma} + i\gamma)$, and the off-diagonal elements $\mathcal{H}_{3j+\sigma-1, 3k+\tau-1} = \xi \mathcal{G}_{\sigma\tau}^{(jk)}$ for $j \neq k$ represent dipole–dipole interactions between different atoms.

2.2 Collective excitation eigenmodes

The dynamics of the atomic ensemble can be understood in terms of the collective excitation eigenmodes \mathbf{v}_n of \mathcal{H} . The eigenvalues $\lambda_n = \delta_n + i\nu_n$ give the collective resonance line shift δ_n and linewidth ν_n [38–42], with $\nu_n < \gamma$ ($\nu_n > \gamma$) defining subradiant (superradiant) modes.

The eigenvectors of the non-Hermitian \mathcal{H} are not orthogonal in general, but satisfy a biorthogonal relationship between the right eigenvectors \mathbf{v}_n , $\mathcal{H} \mathbf{v}_n = \lambda_n \mathbf{v}_n$, and the left eigenvectors, defined by $\mathbf{w}_m^{\dagger} \mathcal{H} = \lambda_m \mathbf{w}_m^{\dagger}$. If \mathcal{H} is diagonalizable, then we can write [4]

$$\mathcal{H} = \sum_n \lambda_n \mathbf{v}_n \mathbf{w}_n^{\dagger}. \quad (6)$$

The eigenvectors obey $\mathbf{w}_n^{\dagger} \mathbf{v}_m = \delta_{nm}$, but $\mathbf{v}_n^{\dagger} \mathbf{v}_m \neq \delta_{nm}$ in general. The mean Petermann factor [4, 43],

$$K = \frac{1}{M} \sum_{m=1}^M (\mathbf{w}_m^{\dagger} \mathbf{w}_m) (\mathbf{v}_m^{\dagger} \mathbf{v}_m), \quad (7)$$

¹ Here the quickly varying terms $\exp(i\omega t)$ have been filtered out such that the amplitudes refer to the slowly varying, positive frequency components.

is an important single measure of the nonorthogonality of an $M \times M$ matrix, with $K = 1$ for Hermitian matrices. The overlap between right eigenvectors is bounded by [4]

$$|\mathbf{v}_n^\dagger \mathbf{v}_m|^2 \leq \frac{4\gamma_n \gamma_m}{(\delta_n - \delta_m)^2 + (\gamma_n + \gamma_m)^2}, \quad (8)$$

and so at degenerate points $\lambda_n = \lambda_m$ it is possible to have an EP where two or more eigenvectors coalesce completely and become linearly dependent. The overlap between left eigenvectors appearing in Equation (7) is not bounded, and at these points K diverges.

At such points, the right eigenvectors no longer form a basis, and \mathcal{H} cannot be diagonalized. It can, however, be expressed in Jordan normal form with eigenvalues on the diagonal, and ones or zeros on the superdiagonal. The solution of a homogeneous undriven ($\mathbf{f} = 0$) set of linear equations (5) is $\mathbf{b}(t) = \exp(i\mathcal{H}t)\mathbf{b}(0)$. Only when the matrix \mathcal{H} can be diagonalized the dynamics separates into independent exponential evolution of each mode. The explicit form of $\exp(i\mathcal{H}t)$ (Supplementary material) contains terms which are linear or higher order in time, depending on the degree of the degeneracy, in addition to an overall exponential dependence.

In the absence of Zeeman splitting, the atomic level structure is isotropic, and \mathcal{H} , while non-Hermitian, is symmetric. In this case the left and right eigenmodes are related by $\mathbf{w}_j^\dagger = \mathbf{v}_j^T$, and so $\mathbf{v}_j^T \mathbf{v}_k = 0$ for $j \neq k$. While modes with $\mathbf{v}_j^T \mathbf{v}_j = 0$ are possible, we can always choose a basis such that $\mathbf{v}_j^T \mathbf{v}_k = \delta_{jk}$ and can then define an occupation measure of the j th mode [34],

$$L_j = \frac{|\mathbf{v}_j^T \mathbf{b}|^2}{\sum_k |\mathbf{v}_k^T \mathbf{b}|^2}. \quad (9)$$

We find in Section 2.3 that, while \mathbf{v}_j are no longer eigenmodes of the full system when Zeeman splitting is turned on, it is still useful to describe the physics in this basis of eigenmodes of the unperturbed system.

There are two collective modes of the unperturbed system that can describe the optical response of the array [34]. They correspond to uniform excitations where the dipoles oscillate in phase and point either in the plane (in-plane mode \mathcal{P}_I), or perpendicular to the plane (out-of-plane mode \mathcal{P}_P). The collective line shifts, shown in Figure 1(a), are generally distinct, but intersect at $d = 0.54\lambda$, where $\delta_{I,P} = -0.71\gamma$. For subwavelength spacing $d < \lambda$, light can only be scattered in the single zeroth-order Bragg peak in the forward or backward direction. When the dipoles point in-plane they can radiate in these directions, and so

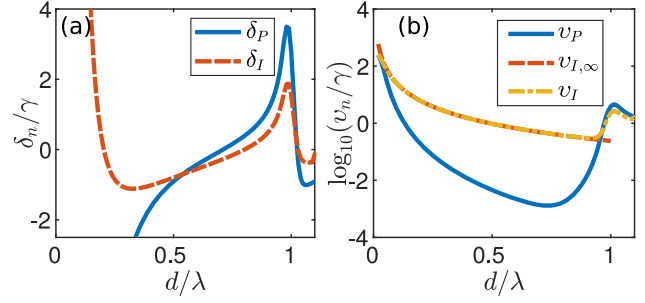


Figure 1: Collective excitation eigenmode (a) line shifts and (b) (log-scale) linewidths of the uniform mode with dipoles pointing out-of-plane (δ_P, ν_P) and in-plane (δ_I, ν_I) for a 20×20 lattice. $\nu_{I,\infty}$ is the $N \rightarrow \infty$ analytic formula [Equation (10)] for ν_I . Resonance level shifts are equal for $d \approx 0.54\lambda$.

the linewidth never substantially narrows [Figure 1(b)]. In the infinite-lattice limit for $d < \lambda$, we find [44, 45]

$$\nu_{I,\infty} \equiv \lim_{N \rightarrow \infty} \nu_I = \frac{3\lambda^2 \gamma}{4\pi d^2}, \quad (10)$$

with this approximation already within 1% of the numerically calculated value for $N \gtrsim 10 \times 10 = 100$.

The collective in-plane excitation eigenmode has now been experimentally observed [20], with all atoms oscillating coherently in phase in an optical lattice of ^{87}Rb atoms with $d = 532 \text{ nm}$ and near unity filling fraction. According to Equation (10), this spacing with $d = 0.68\lambda$ represents a subradiant collective state, resulting in a measured transmission linewidth $\approx 0.66\gamma$, well below the single-atom linewidth. Experiments on illuminating atoms also in optical tweezer arrays are ongoing [46].

In the out-of-plane mode the dipoles radiate predominantly sideways, away from the dipole axis, and light is scattered many times before it can escape from the edges of the lattice. This leads to a dramatically narrowed linewidth with the mode becoming completely dark for large arrays, $\lim_{N \rightarrow \infty} \nu_P = 0$, falling off as $\nu_P \propto N^{-0.9}$ [34].

2.3 Zeeman shifts and two-mode model

The in-plane mode with a uniform phase profile can easily be excited by a wave incident in the x direction normal to the plane, as also shown experimentally [20]. Deeply subradiant modes, with $\nu_n \ll \gamma$, are in general much harder to excite. In the case of the out-of-plane mode the dipoles point perpendicular to the plane, orthogonal to the polarization of a normally incident beam. However, \mathcal{P}_P can be excited by first driving \mathcal{P}_I , and then transferring the

excitation to \mathcal{P}_P by controlling the level shifts [34]. To illustrate this, first consider the effect of level shifts on a single-atom. When the splitting is turned on, the isotropy of the $J = 0 \rightarrow J' = 1$ transition is broken. The amplitudes \mathcal{P}_\pm are driven by the circular light polarizations $\hat{\mathbf{e}}_\pm$ with different resonance frequencies, which in the Cartesian basis appears as coupling between the atomic polarization amplitudes in the x and y directions. The resonances of the single-atom x and y component responses are shifted by an overall average detuning $\tilde{\delta} = \Delta_0 - (\Delta_+ + \Delta_-)/2$, while the splitting between the $\sigma = \pm 1$ levels couples the Cartesian components with strength $\bar{\delta} = (\Delta_- - \Delta_+)/2$, causing the dipoles to rotate.

Similarly for the atomic lattice, the collective modes \mathcal{P}_I and \mathcal{P}_P of the unperturbed lattice are no longer eigenmodes of the full system when the level degeneracy is broken and are instead coupled together. The dynamics of the entire atomic response, however, can be well described by a model of only these two coupled modes, in analogy with the single-atom case [34],

$$\begin{pmatrix} \dot{\mathcal{P}}_I \\ \dot{\mathcal{P}}_P \end{pmatrix} = iH_0 \begin{pmatrix} \mathcal{P}_I \\ \mathcal{P}_P \end{pmatrix} + \begin{pmatrix} f \\ 0 \end{pmatrix}, \quad (11)$$

$$H_0 = \begin{pmatrix} \tilde{\delta}_I + i\nu_I & -i\bar{\delta} \\ i\bar{\delta} & \tilde{\delta}_P + i\nu_P \end{pmatrix},$$

where $\tilde{\delta}_{I,P} = \Delta_0 + \delta_{I,P} - \tilde{\delta}$ and $f = i\epsilon_0 \xi \mathcal{E}/\mathcal{D}$. Here, the incident light directly drives only \mathcal{P}_I , but the level shift contribution $\bar{\delta}$ couples it indirectly to \mathcal{P}_P .

The applicability of the two-mode model follows from the absence of coupling to all other collective modes due to phase mismatching. Figure 2 shows the accuracy of the effective two-mode model in a reflection lineshape of a Gaussian input beam from a 30×30 array, exhibiting a narrow Fano resonance and variation between complete

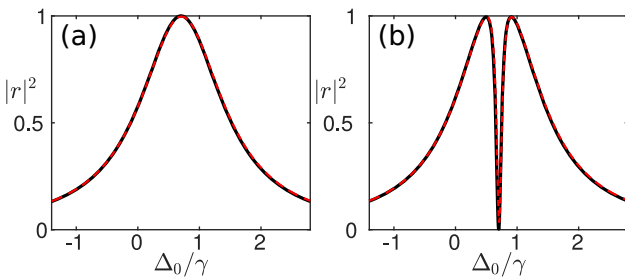


Figure 2: Accuracy of the two-mode model. Reflectance from a 30×30 lattice calculated from two-mode model (full black line) and full numerics (dashed red line) for (a) $\bar{\delta} = 0$ where \mathcal{P}_I is excited on resonance at $\Delta_0 = 0.71\gamma$ leading to total reflection and (b) $\bar{\delta} = 0.2\gamma$ where \mathcal{P}_P is excited, leading to full transmission, with $d = 0.54\lambda$, $\tilde{\delta} = 0$, for Gaussian input with $1/e^2$ radius $w = 12d$. Two-mode model uses parameters $\tilde{\delta}_{P,I} = -0.71$, $\nu_P = 0.003$, $\nu_I = 0.83$ extracted from numerical calculation.

transmission and total reflection [34]. The reflection amplitude is given by

$$r = \frac{\hat{\mathbf{e}}_y \cdot \mathbf{E}_S(-\hat{\mathbf{e}}_x)}{\mathcal{E}} \simeq \frac{i\nu_I Z_P}{\bar{\delta}^2 - Z_I Z_P}, \quad (12)$$

where $\mathbf{E}_S(-\hat{\mathbf{e}}_x)$ is the scattered field in the backward direction and the second expression is the solution of the two-mode model (11) with $Z_{I,P} = \tilde{\delta}_{I,P} + i\nu_{I,P}$. As the laser frequency is tuned through the resonance δ_I of the in-plane mode for zero Zeeman shifts [Figure 2(a)], the atoms fully reflect the light on resonance; a well-known result for dipolar arrays [47] and strongly influenced by collective responses [34, 44, 48–50]. Figure 2(b) shows the case where $\bar{\delta}^2 \gg \nu_P \nu_I$, leading to excitation of \mathcal{P}_P and full transmission, as this mode cannot scatter in the forward or backward direction. A sharp Fano resonance is due to the subradiant \mathcal{P}_P , with the collective modes reminiscent of the dark and bright states in EIT [35], allowing light to be stored in the dark mode [24, 34, 45]. The occupation measure L in Equation (9) for the in-plane mode is as high as 0.99 for the Gaussian input beam considered here [45].

3 Nonexponential decay

As a first example of the physics of EPs, we consider such points away from \mathcal{PT} symmetric regions of the parameter space. We analyze the many-body dynamics of strongly coupled arrays of atoms due to light-mediated interactions that exhibits EPs, also considering the corresponding effective two-mode model. We set $d = 0.54\lambda$ such that $\delta_I = \delta_P$ and $\Delta_0 = -\delta_{I,P}$, resulting in the resonance of both modes being at $\tilde{\delta}_{I,P} = -\tilde{\delta} = 0$. According to the two-mode model, the uniform collective eigenmodes then coalesce at the point $\bar{\delta}^2 = \bar{\nu}^2$, where $\bar{\nu} = (\nu_I - \nu_P)/2$, at which point H_0 has only one right eigenvector. In this case, the eigenvalues of H_0 are complex on both sides of the EP, but the EP itself can be identified by a change in the decay of the polarization amplitudes in the absence of drive. While we predominantly consider polarization dynamics in the limit of low-intensity coherent drive, it is worth noting that this nonexponential decay also applies exactly to the decay of a single-photon quantum excitation [24].

Figure 3(a) shows the decay of an initial state $\mathcal{P}_P = -\mathcal{P}_I$ in the absence of drive for a 20×20 lattice, for varying values of $\bar{\delta}$, with an overall exponential decay $e^{-2\tilde{\nu}t}$, for $\tilde{\nu} = (\nu_I + \nu_P)/2$, factored out. The two-mode model has an EP at $\bar{\delta} \simeq 0.41\gamma$. We find that close to this value the two collective modes of the full lattice become very similar,

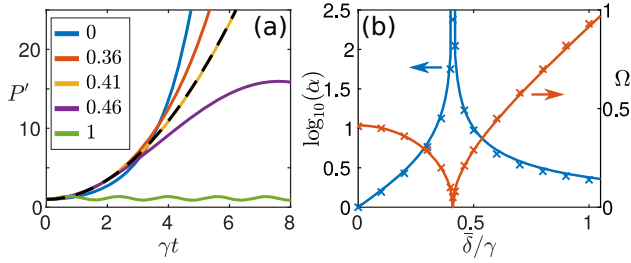


Figure 3: Nonexponential decay at EP of a 20×20 lattice with $d = 0.54\lambda$. (a) $P' = e^{2\tilde{\nu}t}P$, with the survival probability $P = \sum |\mathcal{P}_\sigma^{(j)}|^2$ of a single-photon excitation from initial steady state $\mathcal{P}_I = -\mathcal{P}_P = 1/\sqrt{2}$, for various $\bar{\delta}/\gamma$ given in legend. Black dashed line gives the nonexponential behavior at the EP $\bar{\delta} \approx 0.41\gamma$ of the corresponding two-mode model, dividing real-exponential and oscillatory, complex-exponential contributions. (b) α and Ω extracted from fit of numeric decay (crosses) to Equation (13), and predicted from two-mode model (lines). The EP is characterized by diverging α and $\Omega \rightarrow 0$.

although the limits of numerical accuracy mean they remain distinguishable, and it also marks a transition in the remaining contribution to the decay from real-exponential growth to a complex-exponential, oscillatory form. Close to the transition point, this contribution is approximately quadratic in t , as illustrated by the black, dashed quadratic curve.

The behavior as we transition through the EP is well described by the two-mode model (11) that yields

$$P = |\mathcal{P}_P|^2 + |\mathcal{P}_I|^2 = \exp(-2\tilde{\nu}t) [\cos^2(\Omega t) + \alpha \sin^2(\Omega t)], \quad (13)$$

with $\alpha = (\bar{\delta} + \bar{\nu})/(\bar{\delta} - \bar{\nu})$ and $\Omega = \sqrt{\bar{\delta}^2 - \bar{\nu}^2}$. As $\bar{\delta}$ is varied through the EP $\bar{\delta}^2 = \bar{\nu}^2$, Ω transitions from real to imaginary, and the term in square brackets goes between oscillatory $\sim e^{\pm i|\Omega|t}$, and exponential growth and decay $\sim e^{\pm|\Omega|t}$. Between these two regimes at the EP is nonexponential behavior, characterized by $\alpha \rightarrow \infty$, $\Omega \rightarrow 0$, with $\alpha\Omega^2 \rightarrow 4\bar{\nu}^2$ remaining finite. Only the leading order, nonexponential contribution $1 + \alpha\Omega^2 t^2$ in Equation (13) survives. This limit matches the expected nonexponential solution exactly at the EP;

$$\begin{aligned} \mathcal{P}_- &= \mathcal{P}_-(0) \exp(-\tilde{\nu}t) \\ \mathcal{P}_+ &= \mathcal{P}_+(0) \exp(-\tilde{\nu}t) - 2\tilde{\nu}t\mathcal{P}_-(t), \end{aligned}$$

where $\mathcal{P}_\pm = (\mathcal{P}_I \pm \mathcal{P}_P)/\sqrt{2}$.

The solution of the full many-atom lattice dynamics similarly approaches the nonexponential solution at the EP, as higher-order terms in the exponential expansion are suppressed to longer and longer times (see Supplementary material for more details). Figure 3(b) shows the parameters extracted from fitting the full numeric simulation to the form predicted by Equation (13), with $\Omega \rightarrow 0$ and α

diverging at the EP, as expected. The mean Petermann factor calculated from the two-mode model,

$$K = \frac{1}{2} \left(1 + \frac{\bar{\delta}^2 + \bar{\nu}^2}{|\bar{\delta}^2 - \bar{\nu}^2|} \right), \quad (14)$$

also diverges at this point.

4 \mathcal{PT} symmetry and CPA

While nonexponential decay demonstrates a physical effect of EPs even in the absence of \mathcal{PT} symmetry, EPs are of particular interest when they coincide with the spontaneous breaking of such a symmetry, resulting in a transition of the eigenvalues from purely real to complex. In this section we show how an effective \mathcal{PT} symmetry can arise, when scattering from the collective bright in-plane mode balances loss from the collective dark out-of-plane mode, and how this symmetry can be described by the two-mode model. At the EPs where this symmetry is spontaneously broken, solutions emerge which exhibit CPA, where all coherent transmission and reflection disappears.

4.1 Lattice transmission and scattering

Large arrays can respond collectively as a whole to incoming light normal to the lattice and the atomic excitations exhibit uniform phase profiles. The amplitudes of the incoming and outgoing (transmitted and reflected) fields, as well as each of these and the mode amplitudes are then related by linear transformations in the limit of low light intensity. This leads to quasi-1D physics, where transmission through even several stacked 2D arrays can be treated as a 1D process with each lattice responding as a single “superatom” with a collective resonance line shift and linewidth [45, 51]. Here we show how to prepare an array in a CPA phase that corresponds to the coherently scattered field perfectly canceling the external field, leading to no outgoing coherent light.

For zero Zeeman shifts, we can rewrite the equations of motion (11) in terms of the scalar amplitude of the y component of the uniform mode for a single planar array j

$$\partial_t \mathcal{P}_I^{(j)} = \left(i\tilde{\delta}_I - \nu_I \right) \mathcal{P}_I^{(j)} + \frac{2i\nu_I}{\bar{D}k} \epsilon_0 E_{\text{ext}}^{(j)}, \quad (15)$$

where $\bar{D} = \mathcal{D}/\mathcal{A}$ denotes the density of atomic dipoles on the array for $\mathcal{A} = d^2$, the element of the square unit cell, and we have used ν_I from Equation (10). For a large ideal 2D subwavelength array, only the in-plane mode scatters light

coherently in the exact forward and backward directions. The field scattered by a planar array located at x_j can then be approximated at x , where the distance from the array satisfies $\lambda \leq |x - x_j| \ll \sqrt{\mathcal{A}}$, by the field scattered from a uniform slab [45, 51, 52]. The total field is then the sum of the incident and the scattered fields

$$E(\mathbf{r}) = \mathcal{E}e^{ikx} + \frac{ik\tilde{D}}{2\epsilon_0}e^{ik|x-x_j|}\mathcal{P}_I^{(j)}, \quad (16)$$

indicating that only the average dipole moment per unit area is important. This system corresponds to 1D scalar electrodynamics, and with the average dipole density \mathcal{D}/d^2 , the linewidth of the in-plane mode \mathcal{P}_I equals the effective 1D linewidth $\gamma_{1D} = 3\pi\gamma/(k^2\mathcal{A})$ [53]. The 3D dipole radiation kernel, Equation (3), has now been replaced by the one from 1D electrodynamics $(ik/2)e^{ik|x-x_j|}$ which also represents the interaction between uniformly excited planar arrays at different x positions. This is equivalent to dipole-dipole coupled atoms interacting via a 1D waveguide [45, 51] (see Supplementary material).

Here, we consider the response of an individual lattice plane to a general external field and drop the label j . We separate the fields according to the propagation direction $E_{\text{ext}} = E_{\text{ext}}^{(+)} + E_{\text{ext}}^{(-)}$, with $E_{\text{ext}}^{(\pm)}$ denoting the amplitude of the external field coming *toward* the array from the $\pm x$ direction.² The total field *outgoing* from the array to the $\pm x$ direction is

$$E^{(\pm)} = E_{\text{ext}}^{(\pm)} + \eta(E_{\text{ext}}^{(+)} + E_{\text{ext}}^{(-)}). \quad (17)$$

The second term denotes the scattered light $E_s^{(\pm)} = \eta(E_{\text{ext}}^{(+)} + E_{\text{ext}}^{(-)})$ that is equal in both directions and depends only on the total field at the array. The coefficient $\eta = ik\alpha/2$ can be derived by noting that, aside from the propagation phase factor, $\epsilon_0 E_s = (ik\tilde{D}/2)\mathcal{P}_I$ [Equation (16)], while $\tilde{D}\mathcal{P}_I = \alpha\epsilon_0 E_{\text{ext}}$ is determined by the 1D polarizability α from the steady state of Equation (15),

$$\alpha = -\frac{2\nu_I}{k(\tilde{\delta}_I + i\nu_I)}. \quad (18)$$

While an ideal lattice scatters light coherently, incoherent scattering can arise due to fluctuations in the atomic positions, quantum correlations, or defects in the lattice. In the following section, we consider a specific numerical example of incoherent light scattering due to position fluctuations. We now take Equation (17) to refer only the coherent contribution to light. Incoherently scattered light

reduces the coherently scattered amplitude, the second term of Equation (17), and to incorporate this change, we replace η by η' in Equation (17). We then write η'/η as the ratio of the radiative linewidths for the coherent, denoted by ν_I^c , and total scattering (coherent plus incoherent), denoted by ν_I' ,

$$\eta' = \frac{\nu_I^c \eta}{\nu_I'}, \quad (19)$$

indicating that the intensity of the coherent scattering is a fraction $|\nu_I^c/\nu_I'|^2$ of the total. Consider next the steady-state versions ($\dot{\mathcal{P}}_I = \dot{\mathcal{P}}_P = 0$) of Equation (11), with the linewidths replaced by the primed ones $\nu_{I,P}'$ that include the incoherent contributions,

$$\begin{pmatrix} i\nu_I' - \tilde{\delta} & -i\tilde{\delta} \\ i\tilde{\delta} & i\nu_P' - \tilde{\delta} \end{pmatrix} \begin{pmatrix} \mathcal{P}_I \\ \mathcal{P}_P \end{pmatrix} = -\frac{2\nu_I^c \epsilon_0}{\tilde{D}k} \begin{pmatrix} E_{\text{ext}} \\ 0 \end{pmatrix}, \quad (20)$$

where the equation for \mathcal{P}_I is first transformed as in Equation (15) (again we set $\delta_I = \delta_P = -\Delta_0$ and include any additional detuning offset in $\tilde{\delta}$). From Equation (17), together with replacing η by η' , we can substitute $E_{\text{ext}} = E_{\text{ext}}^{(+)} + E_{\text{ext}}^{(-)} = E^{(+)} + E^{(-)} - 2\eta'(E_{\text{ext}}^{(+)} + E_{\text{ext}}^{(-)})$ on the right-hand-side of Equation (20). As we are interested in the total coherent outgoing field and under which conditions this is zero, we rearrange the terms such that only this contribution appears on the right side,

$$(H_T - \tilde{\delta}_{\text{II}}) \begin{pmatrix} \mathcal{P}_I \\ \mathcal{P}_P \end{pmatrix} = -\frac{2\nu_I^c \epsilon_0}{\tilde{D}k} \begin{pmatrix} E^{(+)} + E^{(-)} \\ 0 \end{pmatrix}, \quad (21)$$

where

$$H_T = \begin{pmatrix} i\nu_I' - 2i\nu_I^c & -i\tilde{\delta} \\ i\tilde{\delta} & i\nu_P' \end{pmatrix}. \quad (22)$$

The difference between this and the evolution matrix H_0 in Equation (11) is that the scattered light is expressed in terms of the mode amplitudes on the left-hand-side of Equation (21) (the $2i\nu_I^c$ term), representing passive gain due to incident light. Parity inversion and time reversal correspond to an interchange of the two modes and complex conjugation, respectively. While H_0 in Equation (11) cannot exhibit \mathcal{PT} symmetry for $\nu_{I,P}' > 0$, the matrix H_T is invariant under this symmetry if $2\nu_I^c - \nu_I' = \nu_P'$, which is possible when $\nu_I^c > \nu_I'/2$. When this symmetry is satisfied, i.e., when the net coherent scattering of light from the bright, in-plane mode balances the loss due to incoherent scattering from the dark, out-of-plane mode, the matrix H_T is \mathcal{PT} symmetric. The eigenvectors of H_T coalesce at an EP at $\tilde{\delta}^2 = (\nu_P')^2 = (2\nu_I^c - \nu_I')^2$. While the matrix retains the \mathcal{PT} symmetry regardless of the value of $\tilde{\delta}$, it is at this point that

² All the fields refer to the positive frequency components.

the eigenmodes themselves transition to being no longer invariant under the \mathcal{PT} operation.

The scattering matrix S links the total outgoing fields to the incoming fields and can also be directly derived from Equation (17), or alternatively from Equation (21). Written in terms of the complex reflection amplitude r and transmission amplitude t , S is defined as

$$\begin{pmatrix} E^{(+)} \\ E^{(-)} \end{pmatrix} = S \begin{pmatrix} E_{\text{ext}}^{(-)} \\ E_{\text{ext}}^{(+)} \end{pmatrix} = \begin{pmatrix} t & r \\ r & t \end{pmatrix} \begin{pmatrix} E_{\text{ext}}^{(-)} \\ E_{\text{ext}}^{(+)} \end{pmatrix}. \quad (23)$$

It follows that

$$\det S \propto \frac{\det(H_T - \tilde{\delta}\mathbb{I})}{\det H_0}, \quad (24)$$

and so when $\det(H_T - \tilde{\delta}\mathbb{I}) = 0$, which is possible only when H_T has a real eigenvalue $\tilde{\delta}$, the scattering matrix S has a zero eigenvalue. Physically, this implies there is a combination of incident light which is completely absorbed, leading to zero coherent outgoing field. At the EPs, the eigenvalues of H_T transition from fully real to complex conjugate pairs, as the \mathcal{PT} symmetry is spontaneously broken. When the eigenvalues are real, CPA is possible. As the scattered field in both directions is equal, full destructive interference can only occur on both sides if the incident field is also symmetric, and so the eigenvalue which goes to zero must be $t + r$, corresponding to $E_{\text{ext}}^{(+)} = E_{\text{ext}}^{(-)}$.

4.2 Tuning collective mode linewidths

As shown in the previous section, \mathcal{PT} symmetry can be achieved when $2\nu_f^c - \nu_l^i = \nu_p^r$. For an ideal lattice with fixed atomic positions $\nu_p \ll \nu_l$. However, while the atoms remain in the ground state of the trap, the wavefunction in this state has a finite size. We model a finite optical lattice with depth sE_R , in units of the lattice photon recoil energy $E_R = \pi^2 \hbar^2 / (2md^2)$, by stochastically sampling the atomic positions from the harmonic oscillator Gaussian density distribution at each site, with root-mean-square width $l = ds^{-1/4}/\pi$, over many realizations [37]. Then fluctuations in the atomic positions will both increase ν_p^r , and tune the rate ν_f^c of coherent scattering. The total outgoing power, $P = P_c + P_{\text{inc}}$, has coherent contributions arising from interference between the incoming light and the average scattered field,

$$P_c = 2\epsilon_0 c \int dS |\mathcal{E} + \langle \mathbf{E}_s \rangle|^2, \quad (25)$$

and incoherent contributions due to fluctuations,

$$P_{\text{inc}} = 2\epsilon_0 c \int dS (\langle \mathbf{E}_s^\dagger \cdot \mathbf{E}_s \rangle - |\langle \mathbf{E}_s \rangle|^2), \quad (26)$$

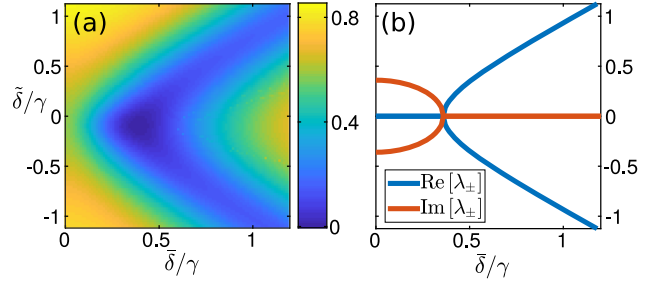


Figure 4: Emergence of CPA due to \mathcal{PT} symmetry breaking. (a) Intensity $|t+r|^2$ of total coherent outgoing light for symmetric incident light showing the emergence of two real detunings corresponding to CPA. (b) Real part (blue) and imaginary part (orange) of eigenvalues of matrix H_T in Equation (22) (in units of γ), showing bifurcation at the EP $\bar{\delta} = (2\nu_f^c - \nu_l^i) = \nu_p^r = 0.4\gamma$, with real eigenvalues corresponding to CPA phase shown in (a).

where the angled brackets represent averaging over many stochastic realizations, and the integral is over the full closed surface [32]. As energy is radiated away, the amplitude decays with an effective scattering linewidth $\nu \propto P$. Incoherent scattering from both modes increases with increasing position uncertainty l , while coherent scattering from \mathcal{P}_l decreases. This implies that while ν_p^r increases, the difference $2\nu_f^c - \nu_l^i$ decreases, and the two values approach and become approximately equal leading to an effective \mathcal{PT} symmetry.

We calculate directly the total coherent output intensity, averaged over 1500 stochastic realizations, for a 20×20 lattice under steady-state symmetric Gaussian beam illumination from both sides, with $1/e^2$ radius $8d$, and $l = 0.2d$, corresponding to $s \approx 6.5$. The output intensity, normalized by the total input intensity from both beams, gives $|t+r|^2$, shown in Figure 4(a). For $\tilde{\delta} \approx 0.4\gamma$, approximate CPA emerges, with $|t+r|^2 \approx 0.03$ at the minimum. For larger $\tilde{\delta}$, the CPA phase then splits into two branches. While there is considerable incoherent scattering due to position fluctuations, the total coherent output remains relatively high away from these branches.

Again this behavior is explained by the simple two-mode model. The eigenvalues λ_{\pm} of H_T are shown in Figure 4(b), for $\nu_p^r = 2\nu_f^c - \nu_l^i = 0.4\gamma$, corresponding to the point of maximum absorption in the numerics. At $\tilde{\delta} = \nu_p^r$, there is an EP where the eigenvalues transition from purely imaginary to purely real. Above this point, the CPA phase in the full lattice is seen when $\tilde{\delta}$ matches one of these real eigenvalues, i.e., when $\tilde{\delta}^2 = \bar{\delta}^2 - (\nu_p^r)^2$. Equation (24) then implies that there are real detunings $\tilde{\delta}$ which lead to the zero eigenvalues $t+r=0$, resulting in CPA. K has the same

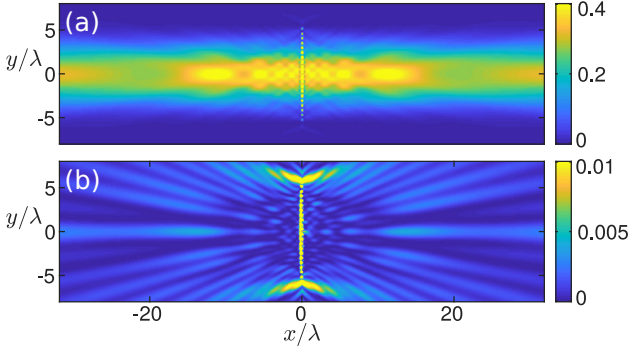


Figure 5: Spatial dependence of intensity for reflecting and CPA phases for a 20×20 atom array on the yz plane at $x=0$. Total outgoing coherent intensity for $\tilde{\delta} = 0$, (a) $\bar{\delta} = 0$, where $|t+r|^2 = 0.6$, and (b) $\bar{\delta} = 0.4$, where $|t+r|^2 = 0.03$, showing CPA, when the atoms are illuminated by Gaussian beams propagating from $\pm x$ directions. Note different color scales. Field is normalized such that $|\mathcal{E}| = 1$ at $x = 0$.

form as Equation (14), with $\bar{\nu}$ being replaced by ν'_p , and diverges at the EP.

The spatial variation of the total coherent outgoing field, for the same lattice parameters and illumination as Figure 4, is shown in Figure 5 for two cases, one where the lattice is strongly reflective, and one where CPA is achieved. In the second case, there is near total cancellation between the coherent scattering and the external field, resulting in a drastic reduction in intensity, with peak intensity around the edge of the lattice.

5 \mathcal{PT} symmetry and polarization conversion

We propose two other realizations of \mathcal{PT} symmetric scattering with atomic arrays. The first, described here, can be achieved by considering scattering between incoming and outgoing light of a single polarization, while treating the orthogonally polarized outgoing light as loss. A final example, where full reflection from the array is described by \mathcal{PT} symmetry, is presented in Supplementary material.

We now consider an array in the xy plane, where the quantization axis remains aligned with the z axis, such that the two in-plane uniform modes, with \mathcal{P}_{Ix} and \mathcal{P}_{Iy} the polarization in the x and y direction, respectively, are coupled. These two modes are degenerate with $\delta_{Ix} = \delta_{Iy} = \delta_I$ and $\nu_{Ix} = \nu_{Iy} = \nu_I$. If we consider the transmission and reflection of only y -polarized light, then any x -polarized scattering can be treated as loss. In the case of an ideal lattice, the modes \mathcal{P}_{Ix} and \mathcal{P}_{Iy} will each scatter light in the respective polarization, with only coherent scattering present, giving $\nu_{Iy}^c = \nu'_{Ix,y} = \nu_I$ and $\nu_{Ix}^c = 0$. We consider

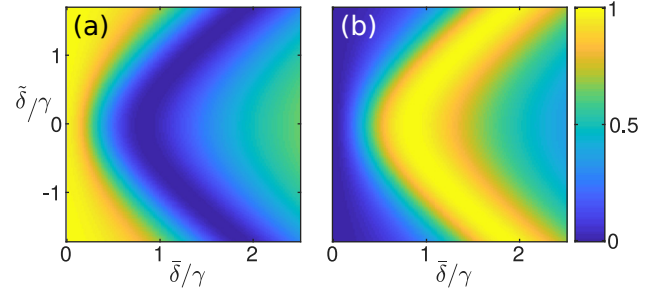


Figure 6: \mathcal{PT} symmetry in polarization conversion. (a) y component $|E_y^{(+)}|^2 + |E_y^{(-)}|^2$ of total outgoing (transmitted and reflected) light leaving the array as a function of $\tilde{\delta}$ and $\bar{\delta}$, and (b) outgoing x polarized light $|E_x^{(+)}|^2 + |E_x^{(-)}|^2$, for symmetric y polarized plane wave incident on 20×20 lattice with $d = 0.54\lambda$. At the EP at $\bar{\delta} = \nu_I$, solutions emerge for which total polarization conversion is possible. EP occurs at $\tilde{\delta} = 0$ and $\bar{\delta} = \nu_I = 0.83\gamma$.

plane wave illumination $\mathcal{E} = \left(E_{\text{ext}}^{(-)} e^{ikz} + E_{\text{ext}}^{(+)} e^{-ikz} \right) \hat{\mathbf{e}}_y$. Due to coupling between the y and x directions, the scattered field will contain both polarization components, such that the total field can be decomposed into $E_x^{(\pm)} = E_{s,x}^{(\pm)}$ and $E_y^{(\pm)} = E_{s,y}^{(\pm)} + E_{\text{ext}}^{(\mp)}$, respectively. Then the mode amplitudes for the y polarization are linked to the field amplitudes, in analogy with Equation (22), through

$$(H_{\text{pol}} - \tilde{\delta}\mathbb{I}) \begin{pmatrix} \mathcal{P}_{I,y} \\ \mathcal{P}_{I,x} \end{pmatrix} = -\frac{2\nu_I \epsilon_0}{\tilde{D}k} \begin{pmatrix} E_y^{(+)} + E_y^{(-)} \\ 0 \end{pmatrix}, \quad (27)$$

where

$$H_{\text{pol}} = \begin{pmatrix} -i\nu_I & -i\bar{\delta} \\ i\bar{\delta} & i\nu_I \end{pmatrix} \quad (28)$$

is automatically \mathcal{PT} symmetric, with EPs at $\bar{\delta}^2 = \nu_I^2$.

Again, this \mathcal{PT} symmetry leads to a zero in the scattering matrix between y -polarized input and output, corresponding to zero outgoing y polarization for two real detunings $\tilde{\delta}$ above the EP. At these points the light is not scattered incoherently, but rather converted completely to the orthogonal x polarization. Figure 6 shows the outgoing intensity in the y and x polarizations for symmetric y -polarized incidence, with perfect coherent polarization conversion emerging above the EP.

6 Conclusion

\mathcal{PT} symmetry has emerged as an important topic in the physics of non-Hermitian systems, as this symmetry can lead to real eigenvalues of the system Hamiltonian. The behavior of a \mathcal{PT} symmetric system can change dramatically at exceptional points, where eigenvectors coalesce

and this symmetry is spontaneously broken. This is in stark contrast to Hermitian systems, where eigenvectors remain orthogonal even at spectral degeneracies.

We have shown how an effective \mathcal{PT} symmetry can arise, without gain, in the many-body dynamics of strongly coupled arrays of atoms due to light-mediated interactions, leading to CPA with almost no coherent transmission or reflection. This symmetry is achieved by balancing the coherent scattering from a bright mode, which couples strongly to incident radiation, with the incoherent scattering from a dark mode, which couples weakly. The \mathcal{PT} symmetry is spontaneously broken at EPs where the eigenmodes coalesce, and the CPA phase emerges, with nonexponential decay at these points. Remarkably, the optical response of arrays of hundreds of atoms can be described by a simple two-mode model, which explains the complete coherent absorption, reflection, and polarization conversion of light, providing a simple and intuitive description. Here, however, the modes in question are collective modes of the entire many-body system, whose properties arise from cooperative interactions and differ dramatically from that of a single atom.

Data used in this publication is available at <https://doi.org/10.17635/lanaster/researchdata/408>.

Author contributions: All the authors have accepted responsibility for the entire content of this submitted manuscript and approved submission.

Research funding: We acknowledge financial support from the UK EPSRC (Grant Nos. EP/S002952/1, EP/P026133/1).

Conflict of interest statement: The authors declare no conflicts of interest regarding this article.

References

- [1] N. I. Zheludev and Y. S. Kivshar, “From metamaterials to metadevices,” *Nat. Mater.*, vol. 11, pp. 917–924, 2012.
- [2] R. El-Ganainy, K. G. Makris, D. N. Christodoulides, and Z. H. Musslimani, “Theory of coupled optical \mathcal{PT} -symmetric structures,” *Opt. Lett.*, vol. 32, pp. 2632–2634, 2007.
- [3] Ş. K. Özdemir, S. Rotter, F. Nori, and L. Yang, “Parity-time symmetry and exceptional points in photonics,” *Nat. Mater.*, vol. 18, pp. 783–798, 2019.
- [4] Y. Ashida, Z. Gong, and M. Ueda, “Non-hermitian physics,” 2020. arXiv:2006.01837 [cond-mat.mes-hall].
- [5] H. Ramezani, T. Kottos, R. El-Ganainy, and D. N. Christodoulides, “Unidirectional nonlinear-symmetric optical structures,” *Phys. Rev. A*, vol. 82, p. 043803, 2010.
- [6] B. Peng, Ş. K. Özdemir, F. Lei, et al., “Parity-time-symmetric whispering-gallery microcavities,” *Nat. Phys.*, vol. 10, pp. 394–398, 2014.
- [7] Z. Lin, H. Ramezani, T. Eichelkraut, T. Kottos, H. Cao, and D. N. Christodoulides, “Unidirectional invisibility induced by \mathcal{PT} -symmetric periodic structures,” *Phys. Rev. Lett.*, vol. 106, p. 213901, 2011.
- [8] L. Feng, Y.-L. Xu, W. S. Fegadolli, et al., “Experimental demonstration of a unidirectional reflectionless parity-time metamaterial at optical frequencies,” *Nat. Mater.*, vol. 12, pp. 108–113, 2013.
- [9] S. Longhi, “ \mathcal{PT} -symmetric laser absorber,” *Phys. Rev. A*, vol. 82, p. 031801, 2010.
- [10] W. Wan, Y. Chong, L. Ge, H. Noh, A. D. Stone, and H. Cao, “Time-reversed lasing and interferometric control of absorption,” *Science*, vol. 331, pp. 889–892, 2011.
- [11] Y. D. Chong, L. Ge, H. Cao, and A. D. Stone, “Coherent perfect absorbers: time-reversed lasers,” *Phys. Rev. Lett.*, vol. 105, p. 053901, 2010.
- [12] C. M. Bender and S. Boettcher, “Real spectra in non-hermitian Hamiltonians having symmetry,” *Phys. Rev. Lett.*, vol. 80, pp. 5243–5246, 1998.
- [13] M.-A. Miri and A. Alù, “Exceptional points in optics and photonics,” *Science*, vol. 363, p. eaar7709, 2019.
- [14] A. Guo, G. J. Salamo, D. Duchesne, et al., “Observation of \mathcal{PT} -symmetry breaking in complex optical potentials,” *Phys. Rev. Lett.*, vol. 103, p. 093902, 2009.
- [15] M. Ornigotti and A. Szameit, “Quasi \mathcal{PT} -symmetry in passive photonic lattices,” *J. Opt.*, vol. 16, p. 065501, 2014.
- [16] M. Kang, F. Liu, and J. Li, “Effective spontaneous \mathcal{PT} -symmetry breaking in hybridized metamaterials,” *Phys. Rev. A*, vol. 87, p. 053824, 2013.
- [17] Y. Sun, W. Tan, H.-Q. Li, J. Li, and H. Chen, “Experimental demonstration of a coherent perfect absorber with \mathcal{PT} phase transition,” *Phys. Rev. Lett.*, vol. 112, p. 143903, 2014.
- [18] N. Yu and F. Capasso, “Flat optics with designer metasurfaces,” *Nat. Mater.*, vol. 13, pp. 139–150, 2014.
- [19] S. D. Jenkins and J. Ruostekoski, “Controlled manipulation of light by cooperative response of atoms in an optical lattice,” *Phys. Rev. A*, vol. 86, p. 031602, 2012.
- [20] J. Rui, D. Wei, A. Rubio-Abadal, et al., “A subradiant optical mirror formed by a single structured atomic layer,” *Nature*, vol. 583, pp. 369–374, 2020.
- [21] S. D. Jenkins, J. Ruostekoski, N. Papasimakis, S. Savo, and N. I. Zheludev, “Many-body subradiant excitations in metamaterial arrays: experiment and theory,” *Phys. Rev. Lett.*, vol. 119, p. 053901, 2017.
- [22] A. S. Solntsev, G. S. Agarwal, and Y. S. Kivshar, “Metasurfaces for quantum photonics,” 2020. arXiv:2007.14722 [physics.optics].
- [23] P.-O. Guimond, A. Grankin, D. V. Vasilyev, B. Vermersch, and P. Zoller, “Subradiant bell states in distant atomic arrays,” *Phys. Rev. Lett.*, vol. 122, p. 093601, 2019.
- [24] K. E. Ballantine and J. Ruostekoski, “Subradiance-protected excitation spreading in the generation of collimated photon emission from an atomic array,” *Phys. Rev. Res.*, vol. 2, p. 023086, 2020.
- [25] M. Hebenstreit, B. Kraus, L. Ostermann, and H. Ritsch, “Subradiance via entanglement in atoms with several independent decay channels,” *Phys. Rev. Lett.*, vol. 118, p. 143602, 2017.

- [26] A. Piñeiro Orioli and A. M. Rey, “Dark states of multilevel fermionic atoms in doubly filled optical lattices,” *Phys. Rev. Lett.*, vol. 123, p. 223601, 2019.
- [27] L. A. Williamson, M. O. Borgh, and J. Ruostekoski, “Superatom picture of collective nonclassical light emission and dipole blockade in atom arrays,” *Phys. Rev. Lett.*, vol. 125, p. 073602, 2020.
- [28] A. Cidrim, T. S. do Espirito Santo, J. Schachenmayer, R. Kaiser, and R. Bachelard, “Photon blockade with ground-state neutral atoms,” *Phys. Rev. Lett.*, vol. 125, p. 073601, 2020.
- [29] R. Bekenstein, I. Pikovski, H. Pichler, E. Shahmoon, S. F. Yelin, and M. D. Lukin, “Quantum metasurfaces with atom arrays,” *Nat. Phys.*, vol. 16, pp. 676–681, 2020.
- [30] K. E. Ballantine and J. Ruostekoski, “Optical magnetism and Huygens’ surfaces in arrays of atoms induced by cooperative responses,” *Phys. Rev. Lett.*, vol. 125, p. 143604, 2020.
- [31] R. Alaei, B. Gurlek, M. Albooyeh, D. Martín-Cano, and V. Sandoghdar, “Quantum metamaterials with magnetic response at optical frequencies,” *Phys. Rev. Lett.*, vol. 125, p. 063601, 2020.
- [32] R. J. Bettles, M. D. Lee, S. A. Gardiner, and J. Ruostekoski, “Quantum and nonlinear effects in light transmitted through planar atomic arrays,” *Commun. Phys.*, vol. 3, p. 141, 2020.
- [33] C. D. Parmee and J. Ruostekoski, “Signatures of optical phase transitions in superradiant and subradiant atomic arrays,” *Commun. Phys.*, vol. 3, p. 205, 2020.
- [34] G. Facchinetti, S. D. Jenkins, and J. Ruostekoski, “Storing light with subradiant correlations in arrays of atoms,” *Phys. Rev. Lett.*, vol. 117, p. 243601, 2016.
- [35] M. Fleischhauer, A. Imamoglu, and J. P. Marangos, “Electromagnetically induced transparency: optics in coherent media,” *Rev. Mod. Phys.*, vol. 77, pp. 633–673, 2005.
- [36] F. Gerbier, A. Widera, S. Fölling, O. Mandel, and I. Bloch, “Resonant control of spin dynamics in ultracold quantum gases by microwave dressing,” *Phys. Rev. A*, vol. 73, p. 041602, 2006.
- [37] M. D. Lee, S. D. Jenkins, and J. Ruostekoski, “Stochastic methods for light propagation and recurrent scattering in saturated and nonsaturated atomic ensembles,” *Phys. Rev. A*, vol. 93, p. 063803, 2016.
- [38] S. D. Jenkins, J. Ruostekoski, J. Javanainen, et al., “Collective resonance fluorescence in small and dense atom clouds: comparison between theory and experiment,” *Phys. Rev. A*, vol. 94, p. 023842, 2016.
- [39] R. T. Sutherland and F. Robicheaux, “Collective dipole–dipole interactions in an atomic array,” *Phys. Rev. A*, vol. 94, p. 013847, 2016.
- [40] A. Asenjo-Garcia, M. Moreno-Cardoner, A. Albrecht, H. J. Kimble, and D. E. Chang, “Exponential improvement in photon storage fidelities using subradiance and “selective radiance” in atomic arrays,” *Phys. Rev. X*, vol. 7, p. 031024, 2017.
- [41] Y.-X. Zhang and K. Mølmer, “Theory of subradiant states of a one-dimensional two-level atom chain,” *Phys. Rev. Lett.*, vol. 122, p. 203605, 2019.
- [42] J. A. Needham, I. Lesanovsky, and B. Olmos, “Subradiance-protected excitation transport,” *New J. Phys.*, vol. 21, p. 073061, 2019.
- [43] K. Petermann, “Calculated spontaneous emission factor for double-heterostructure injection lasers with gain-induced waveguiding,” *IEEE J. Quant. Electron.*, vol. 15, pp. 566–570, 1979.
- [44] S. D. Jenkins and J. Ruostekoski, “Metamaterial transparency induced by cooperative electromagnetic interactions,” *Phys. Rev. Lett.*, vol. 111, p. 147401, 2013.
- [45] G. Facchinetti and J. Ruostekoski, “Interaction of light with planar lattices of atoms: reflection, transmission, and cooperative magnetometry,” *Phys. Rev. A*, vol. 97, p. 023833, 2018.
- [46] A. Glicenstein, G. Ferioli, N. Šibalić, L. Brossard, I. Ferrier-Barbut, and A. Browaeys, “Collective shift in resonant light scattering by a one-dimensional atomic chain,” *Phys. Rev. Lett.*, vol. 124, p. 253602, 2020.
- [47] S. Tretyakov, *Analytical Modeling in Applied Electromagnetics*, 1st ed., Norwood, MA, Artech House, 2003.
- [48] F. J. García de Abajo, “Colloquium: light scattering by particle and hole arrays,” *Rev. Mod. Phys.*, vol. 79, pp. 1267–1290, 2007.
- [49] R. J. Bettles, S. A. Gardiner, and C. S. Adams, “Enhanced optical cross section via collective coupling of atomic dipoles in a 2d array,” *Phys. Rev. Lett.*, vol. 116, p. 103602, 2016.
- [50] E. Shahmoon, D. S. Wild, M. D. Lukin, and S. F. Yelin, “Cooperative resonances in light scattering from two-dimensional atomic arrays,” *Phys. Rev. Lett.*, vol. 118, p. 113601, 2017.
- [51] J. Javanainen and R. Rajapakse, “Light propagation in systems involving two-dimensional atomic lattices,” *Phys. Rev. A*, vol. 100, p. 013616, 2019.
- [52] L. Chomaz, L. Corman, T. Yefsah, R. Desbuquois, and J. Dalibard, “Absorption imaging of a quasi-two-dimensional gas: a multiple scattering analysis,” *New J. Phys.*, vol. 14, p. 005501, 2012.
- [53] J. Javanainen, J. Ruostekoski, B. Vestergaard, and M. R. Francis, “One-dimensional modeling of light propagation in dense and degenerate samples,” *Phys. Rev. A*, vol. 59, pp. 649–666, 1999.

Supplementary Material: The online version of this article offers supplementary material (<https://doi.org/10.1515/nanoph-2020-0635>).